Astron. Astrophys. 230, 445–456 (1990)

ASTRONOMY
AND
ASTROPHYSICS

The kinematic structure of NGC 7139

N. A. Walton [1,2], **J. R. Walsh** [1,3], **and K. C. Sahu** [1,4]

[1] Kapteyn Astronomical Institute, Postbus 800, NL-9700 AV Groningen, The Netherlands
[2] Department of Physics and Astronomy, University College London, Gower Street, London WC1E 6BT, UK
[3] ST-ECF, ESO, Karl-Schwarzschild-Strasse 2, D-8046 Garching bei München, Federal Republic of Germany
[4] Observatorio del Roque de los Muchachos, Apartado 321, Santa Cruz de la Palma (TF), Islas Canarias, Spain

Received May 22, accepted August 17, 1989

Abstract. Spatio-kinematic, seeing limited data, obtained using TAURUS I on the Isaac Newton Telescope, are presented for the northern Galactic planetary nebula NGC 7139 in the emission lines of [O III] 5007 Å and [O I] 6300 Å. Additional low dispersion, long slit, spectra were also taken to obtain information on the central star and the nebular visual spectrum. A three-dimensional model geometrical structure for the nebula was deduced, from which model TAURUS cubes could be derived for comparison with the data. The best fit models have been obtained with a two component structure to describe the PN, namely an optically thick toroidal part and an optically thin (in the Lyman continuum) biconical section. The velocity law is determined as $V = k\,r$ where $k = 165\,\mathrm{km\,s^{-1}\,pc^{-1}}$ for the optically thick part of the nebula and $k = 410\,\mathrm{km\,s^{-1}\,pc^{-1}}$ for the optically thin biconical section of the nebula, assuming a distance of 1.5 kpc to the nebula. The velocity laws indicate that the material in the optically thin part of NGC 7139 has been preferentially accelerated. This may be evidence for the "fast" wind from the central star of NGC 7139 interacting with a non-spherically symmetric wind from the precursor of the planetary nebulae. Alternative explanations are considered.

Key words: planetary nebulae – NGC 7139

1. Introduction

The internal dynamics of a planetary nebula (PN) is the main factor dictating its structure and evolution, and hence is the key to the understanding of the observed form of the PN. However the internal dynamics of a PN is governed by the way that the stellar envelope is ejected and the forces that subsequently act on this in forming the nebular shell. The large variety of observed forms of PNe suggest that the initial conditions, as well as the forces that subsequently act on the nebular shell, may be different in nature for various PNe.

Previous studies of the kinematic structure of PNe have mainly been based on long slit spectroscopic data, usually giving information on the kinematics along one or two axes. Wilson (1950, 1958) showed that the line splitting decreased with increasing ionisation energy of the ionic species, with high ionisation transitions such as [Ne V] having a line splitting of nearly zero in many PNe. These early results were expanded upon by Weedman (1968) who, by using existing data and new data on non-circular PNe, was able to determine the nebular velocity law, i.e. the variation of velocity as a function of radius from the centre of the nebula. He found that the expansion velocity increased in proportion to the radius. This agreed with the observed variation of expansion velocity with ionisation potential. Individual PN differed only in the slope of the $V(r)$ relationship and the value of the intercept at $r = 0$.

However, it must be noted that the above results applied to a sample of rather regular PNe and are based on limited velocity field information. Recently a few authors have made use of Fabry-Perot interferometers to study high velocity features in somewhat more irregular PNe, e.g. the knots in Abell 30 (Reay and Atherton, 1983) and in NGC 7009 (Reay et al., 1985). Additionally Sabbadin (1984) has compiled expansion velocities for a large number of PNe. He finds an expansion velocity with radius plot broadly in agreement with that of Weedman. Further work has been presented by Balick and co-workers based on CCD and long slit echelle spectra of a number of PN (e.g. Balick, 1987; Balick et al., 1987) A recent review of expansion velocity data published upto 1987 is given by Weinberger (1989).

In general however, the global kinematics of PNe are rather poorly determined. Knowing the complete picture is of vital importance if we are to be able to properly study the nebular shell formation mechanism and thereby gain an understanding of which of the several mechanisms of nebular formation is valid for any particular nebula. With the advent of TAURUS (Atherton et al., 1982), a wide field imaging Fabry-Perot interferometer, it has become possible to study the velocity fields of extended emission line objects and hence PNe.

The kinematical observations described here were made as part of a larger programme to study the internal dynamics of different classes of PNe, e.g. those PNe containing large amounts of dust, those with hot central stars, those having central stars with fast winds as evidenced by P-Cygni profiles, etc. Additionally high velocity structures in the PNe could be searched for. Approximately 20 PNe have now been investigated using TAURUS I on the Isaac Newton Telescope. Data cubes in several lines (i.e. [O I] 6300 Å, [O III] 5007 Å, and Hα) have been obtained for these PNe. In this paper we describe one of the sample nebulae, namely NGC 7139.

NGC 7139 (PK No. 104+7°1) is a northern galactic PN, observed by Balick (1987), who classifies it as middle round. The

Send offprint requests to: N. A. Walton (University College London)

distance to NGC 7139 has been determined by several authors. Pottasch (1981) gives 0.9 kpc. Sabbadin et al. (1985) have presented a compilation of distances to NGC 7139, determined by various authors, these distances being: 1.36, 1.48, 1.47, 0.88, 1.19, 1.81, 1.39, 1.15, 1.35, 1.50, all in kpc. More recently Amnuel et al. (1989) have given a distance of 2.1 kpc, while Weinberger and Ziener (1988) give a distance towards NGC 7139 of 2.4 ± 0.7 kpc, found using the extinction method. Hence it is apparent that the distance towards this nebula is only known to within a factor of 2. The mean distance value of 1.5 kpc is adopted for use in this paper.

Observations of NGC 7139 are rather sparse. Kaler (1976) summarises line strengths for this nebula. These show that NGC 7139 has [O III] 5007 Å and He II 4686 Å emission indicating that this nebula is probably of high excitation class (perhaps 7–8). Data that is presented in later sections of this paper would tend to support this view.

The following sections are arranged as follows. Section 2 details the observations that have been made, both with TAURUS and the Intermediate Dispersion Spectrograph at the Isaac Newton Telescope on La Palma. In Sect. 3 the reduction procedures employed are outlined and results from the observations presented. In Sect. 4 details of the model which we have computed to describe the geometrical structure of NGC 7139 are given. Finally the results and the relevance of the model are discussed in Sect. 5.

2. Observations

2.1. TAURUS

Emission line profiles for [O III] 5007 Å and [O I] 6300 Å at "seeing limited" spatial resolutions across NGC 7139 have been obtained using a wide field imaging Fabry-Perot system, TAURUS I (Atherton et al., 1982). The observations were made using the 2.5 metre Isaac Newton Telescope with the IPCS (Boksenberg, 1972) as the detector, on the nights 24, 26, and 27th June 1988. The pixel size for the [O III] data cube was 0″.58 by 0″.58, whilst for the [O I] cube it was 0″.56 by 0″.56. For the [O III] observation the 250 micron gap etalon was used. A data set of 100 frames of 256×256 pixels spaced by 3.4 km s^{-1} in velocity were recorded. The velocity resolution was ≈ 13 km s^{-1} whilst the spatial "seeing", measured from a field star image, was $\approx 1''.5$. The [O I] data was obtained using the 540 micron etalon. Again 100 frames of 256×256 pixels were recorded, the velocity step being 2.1 km s^{-1}. The velocity resolution was ≈ 8 km s^{-1}, the spatial "seeing" was $\approx 1''.5$. Calibration cubes and ring frames were taken with a neon calibration lamp through a number of interference filters to isolate various lines for calibration purposes.

The integration times per frame were 60 s and 48 s for the [O I] and [O III] data respectively, leading to total integration times of 100 min and 80 min. It might be noted in passing that the coordinates for NGC 7139 given in Acker et al. (1982), were found to be incorrect by a considerable amount. The correct coordinates (B 1950) are; RA: $21^h44^m49^s.1$ and Dec: $+63°33'29''$.

2.2. Low dispersion spectroscopy

NGC 7139 was observed on 3 November 1988 with the 2.5 m Isaac Newton Telescope on La Palma and the Intermediate Dispersion Spectrograph (IDS). A 150 lines mm^{-1} grating, blazed at 5250 Å, was used in first order. The detector was a GEC P8603 CCD, dye coated to improve blue response. The spectral coverage of the CCD was 3200 Å and the region 3200 Å to 5750 Å was usefully covered. One slit position over the nebula was observed at position angle 146° with the slit centre on the nebula central star. The slit length was 246″, so included the full diameter of the nebula and sufficient sky on both sides for sky subtraction. Two observations were obtained: – one with a broad slit (1000 μm, 5″.4) to include all the light of the central star and divided into two 1000 s exposures; one with a narrow slit (255 μm, 1″.4) of exposure time 500 s. The spectrophotometric standard star BD +28°4211 (Stone, 1977) was also observed with a broad slit for 100 s. Sky conditions at the time of observation were not ideal with 2″ seeing and some mist.

3. Reduction and results

3.1. TAURUS

The three-dimensional data arrays created were phase-corrected using the TAURUS calibration package at the Kapteyn Sterrenwacht, Roden, The Netherlands (Mulder et al., 1988). Full details of the procedures used in the calibration of TAURUS data are given in Atherton et al. (1982).

The pixel sizes were obtained by analysing two-dimensional mask arrays. Light from the neon calibration lamp, seen through the 5032 Å filter, was shone through a mask plate, located at the focal plane. This mask consisted of a matrix of pinholes with known separations. By measuring the separation of the light spots in the 2D IPCS data array, and having a knowledge of the focal lengths of the optical components of TAURUS I, it was possible to deduce the pixel size of the data arrays. The effective gapsizes of the two etalons were determined by analysing the three calibration cubes of different neon lines.

After phase correction, data cubes were produced of a number of RA-Dec frames separated in velocity. All further reduction of the TAURUS cubes was performed using the GIPSY data reduction package (Allen et al., 1985). In order to increase the signal-to-noise in each individual RA-Dec frame, and taking account of the fact that the data was oversampled in velocity, every second frame of the data was coadded. This gave frame spacings of ≈ 6.7 km s^{-1} and ≈ 4.2 km s^{-1} for the [O III] and [O I] data cubes respectively. The data are presented in the form of images of the individual RA-Dec frames for the [O III] and [O I] data cubes. In Fig. 1 images of the RA-Dec frames summed over one "free spectral range" of the Fabry-Perot are shown. For the [O III] data this is the equivalent of an image obtained through a narrow band filter having a width of 4.7 Å, and for the [O I] data through one of width 3.6 Å.

Figure 2 shows the channel maps in which [O III] emission is present. Each frame is spaced by 6.7 km s^{-1} with velocities going from red to blue from left to right in the figure. The rest velocity of the nebula is between frames 8 and 9. Figure 3 shows the corresponding channel maps for the case of the [O I] data. For display purposes only, the [O I] data has been resampled in velocity so that each RA-Dec frame is spaced by 6.3 km s^{-1} and again the velocities go from red to blue with the frames going from left to right. Here the zero rest velocity of the nebula is between frames 8 and 9.

At any point in the data cubes a spectrum can be generated. Alternatively the spectrum obtained by placing an aperture of some diameter over any part of the nebula can be produced. In Fig. 8 profiles at several positions in the [O I] and [O III] data cubes are shown. The maximum splitting of the two lines, measured

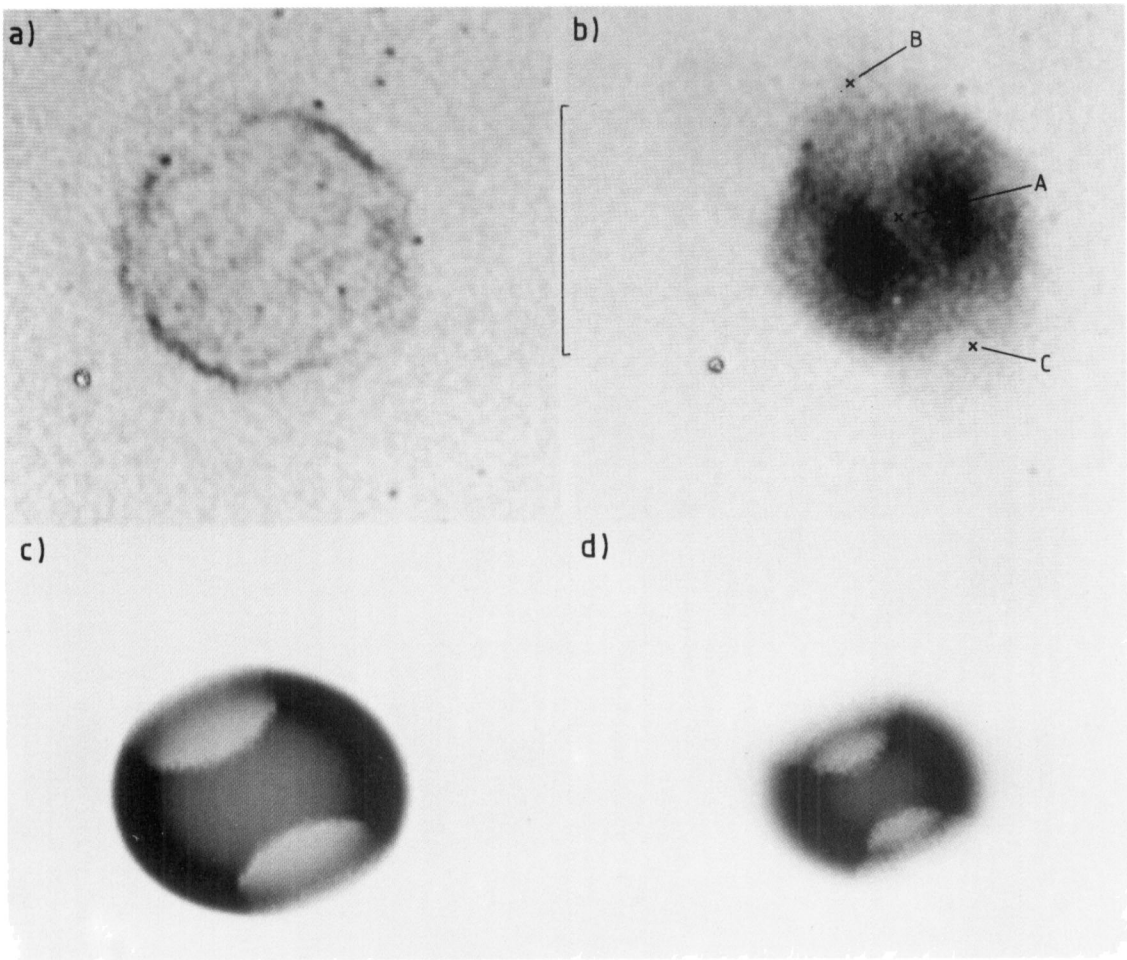

Fig. 1a–d. Plate showing a mosaic of "pseudo" narrow band images of the TAURUS and model data for NGC 7139. In these images North is at the top of the picture and East to the left. A scale bar of 60″ is shown. **a** shows the [O I] image equivalent to a 3.6 Å narrow band image. **b** is the [O III] image equivalent to a 4.7 Å narrow band image. A, B, C mark the centres of the apertures where line profiles were obtained (Fig. 8). **c** shows the model [O I] image where the velocity range over which the model is summed is the same as that for the data and **d** shows the similar model "narrow band image" for [O III]

from the profiles taken through the centre of the nebula, gave the nebula expansion velocity as:

$28 \pm 3\,\mathrm{km\,s^{-1}}$ in [O III]

$38 \pm 3\,\mathrm{km\,s^{-1}}$ in [O I].

The [O III] spectra were compared with the profile in [O III] presented in Weinberger and Ziener (1988). They observed the central 20″ of NGC 7139 with a scanning Fabry-Perot spectrometer and found V_{exp} to be $20\,\mathrm{km\,s^{-1}}$. Using an aperture of 20″ on this TAURUS data a similar value was obtained. This result shows that the measured expansion velocity of a PN is dependant on the size of the aperture used to make the measurement, as has previously been noted by Bohuski and Smith (1974). They found that the observed expansion velocity is a lower limit if the aperture subtends an angle greater that 25% of the mean nebula diameter. It would appear from the above that the expansion velocity must be measured with the smallest aperture possible to give the best estimate of the true expansion velocity.

In Fig. 7 the profile taken through the centre of NGC 7139 in [O I] is shown, this was obtained by integrating over a square aperture of 6″.2 length. The strong lines at $\approx \pm 80\,\mathrm{km\,s^{-1}}$ are due to the [O I] night sky line as seen in different orders of the Fabry-Perot. As can be seen, the nebular line is well separated from the night sky line and is thus not contaminated by it. In passing, it might be noted that the presence of the night sky line within the data cube was of help in the phase correction process, as the phase map could be determined directly from the night sky line.

3.2. Low dispersion spectroscopy

The spectra of NGC 7139 and BD +28°4211 were bias corrected, flat-fielded and wavelength calibrated by exposures to a Cu-Ar comparison lamp. The data were corrected for atmospheric extinction and flux calibrated ($\mathrm{erg\,cm^{-2}\,s^{-1}\,Å^{-1}}$) from the narrow band magnitudes for BD +28°4211 using the FIGARO reduction package. The spectra were sky subtracted employing a mean sky level from both ends of the slit. Figure 5 shows the profiles along the slit of the [O III] 5007 Å and [O II] 3727 Å emission; O^{2+} clearly recombines to O^{+} over the nebula shell. For the broad slit exposure the total spectrum of the nebula (sum of 110 channels along the slit excluding the central star) was formed and the emission lines analysed by summing the flux with a linear

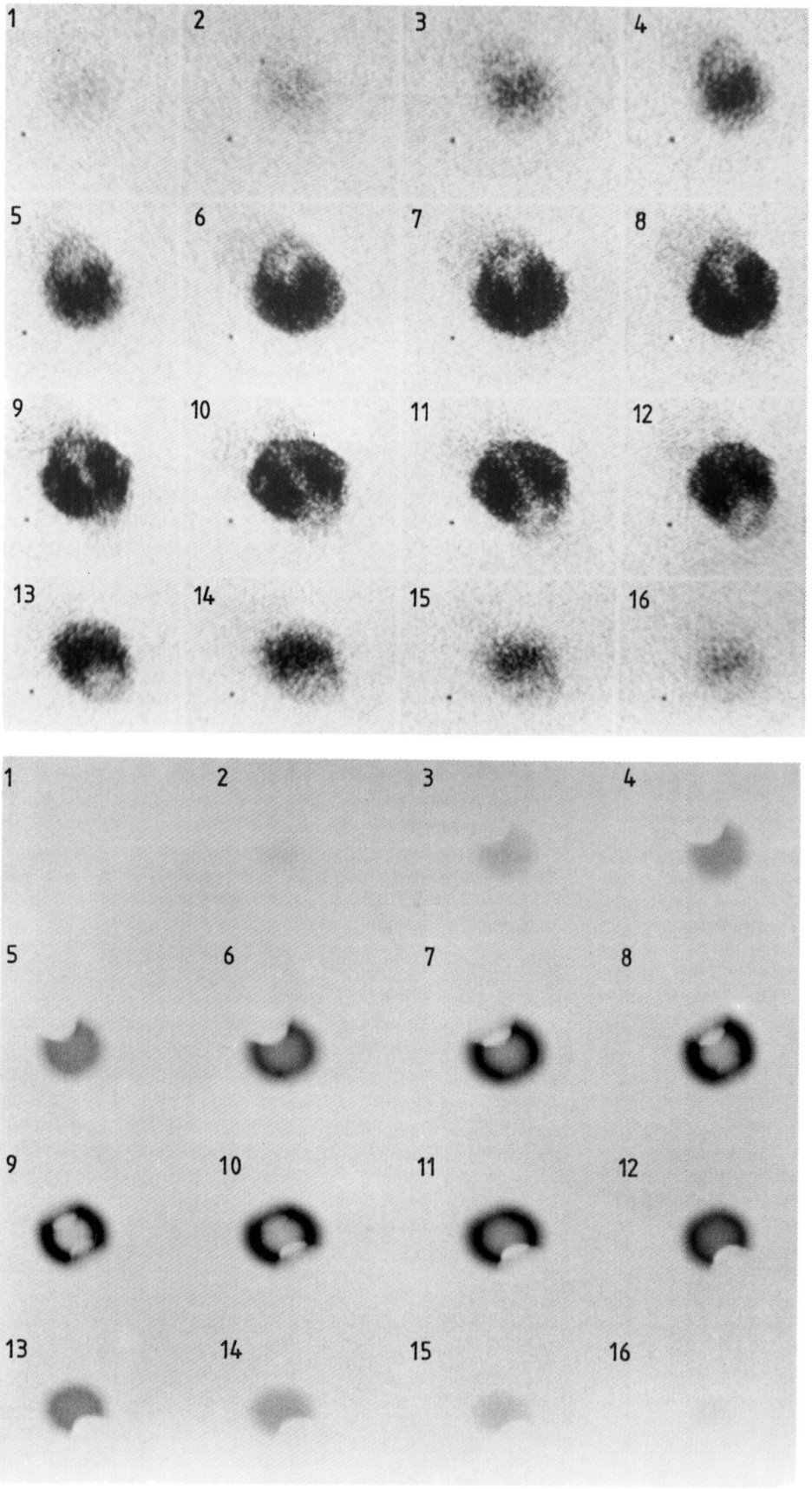

Fig. 2a and b. Plate showing individual velocity frames for **a** the [O III] TAURUS data and **b** the corresponding frames produced from the model. Each frame is spaced by 6.7 km s^{-1} and the frames go from red to blue as you view top left to bottom right. The rest velocity for the [O III] data is between frames 8 and 9

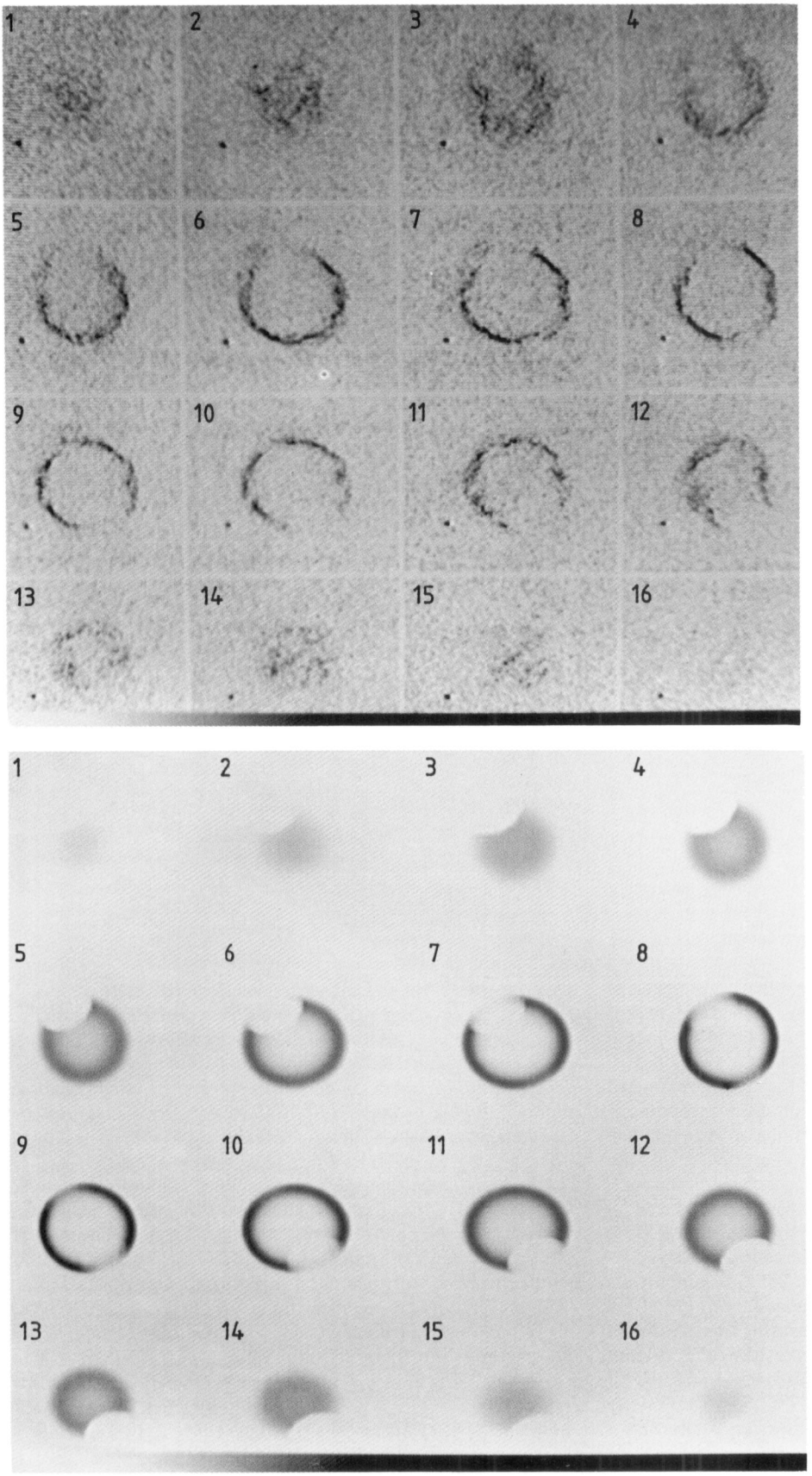

Fig. 3a and b. Plate showing individual velocity frames for **a** the [O I] TAURUS data and **b** the corresponding frames produced from the model. Each frame is spaced by 6.3 km s^{-1} and the frames go from red to blue as you view top left to bottom right. The rest velocity for the [O I] data is between frames 8 and 9

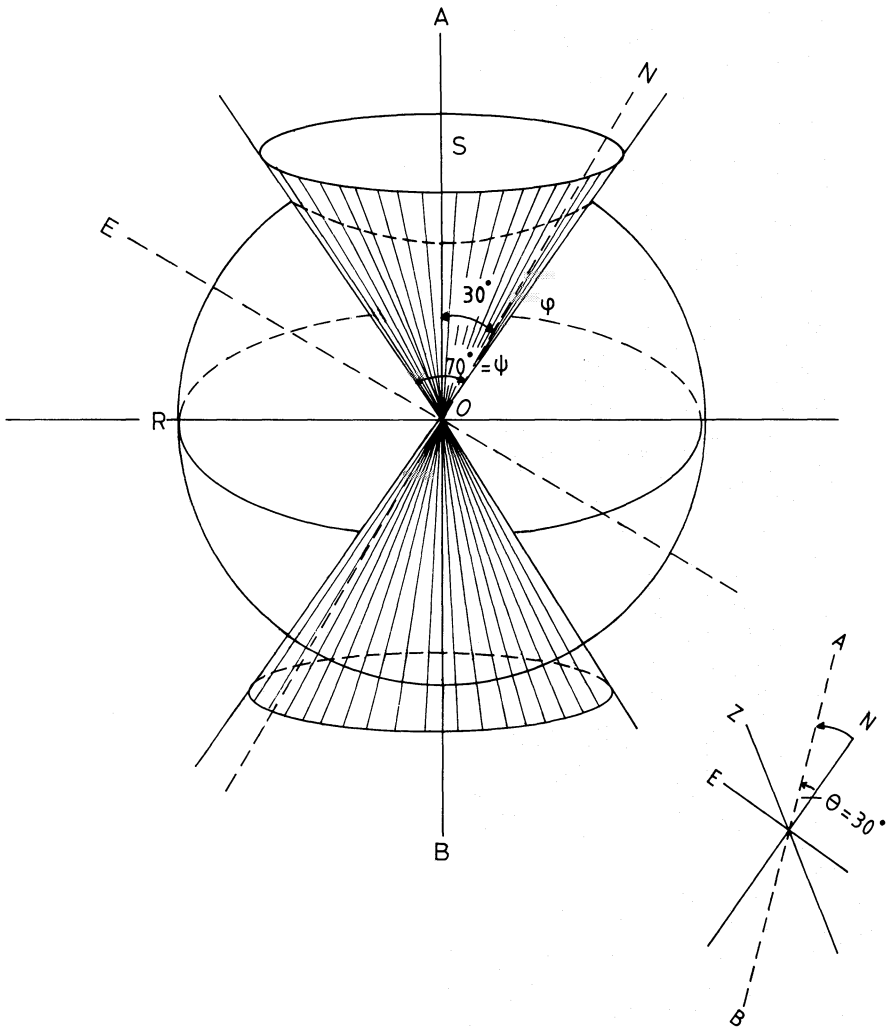

Fig. 4. Schematic representation of the model used for NGC 7139. North and East on the sky are shown. *OR* is the radius of the optically thick part of the nebula, *OS* is the radius of the optically thin part. The main diagram shows the angles ψ and ϕ. The inset diagram shows the angle θ, with the *Z*-axis being into the plane of the sky

interpolation to the continuum under the line. Table 1 presents the observed relative fluxes. The value of the extinction towards NGC 7139 was determined from the ratio of the Hγ to Hβ lines to be $c = 0.6$.

For the broad slit data, the spectrum of the star was extracted (8 channels) and the Hβ emission line flux and the narrow band magnitude at 5450 Å were measured. A simulated *B* magnitude was measured using the method of Jacoby et al. (1984), and the observed *B* magnitude was $m_B = 19.6$. Using $c = 0.6$, and subtracting the nebular continuum, the dereddened magnitude is $m_B = 18.0 \pm 0.25$. For comparison Pilyugin and Khromov (1979) list it's magnitude at *B* to be 18.1 with a large uncertainty.

With the dereddened value for m_B it is possible to compute the temperature of the central star making the assumption that the nebula is optically thick to Lyman-α ionising radiation. To determine the visual flux from the central star, the calibration of Wamsteker (1981) and Tüg et al. (1977) is used – 0 magnitudes in the visual corresponds to $3.64\ 10^{-9}$ erg cm^{-2} s^{-1} Å^{-1}. Kaler and Feibelman (1985) (see also Cahn, 1984) give for a $T = \infty$ star a value for $(B-V)$ of -0.38 mag, leading to a dereddened $m_v = 18.38$ mag. The central star flux, corrected for $c = 0.6$, is then in the visual continuum, $1.62\ 10^{-16}$ erg cm^{-2} s^{-1} Å^{-1}. The recombination line flux emitted in Hβ 4861 Å from NGC 7139 has been measured by O'Dell (1963) as $6.31\ 10^{-12}$ erg cm^{-2} s^{-1}, corrected for $c = 0.6$. The ratio of Hβ flux to visual continuum flux is the $3.899\ 10^4$ Å. This leads to the hydrogen Zanstra temperature of, $T_Z(\mathrm{H}) = 132{,}000$ K.

The helium Zanstra temperature is computed using the above and the ratio He II 4686 Å/Hβ of 0.19 (Kaler, 1976), corrected for reddening with $c = 0.6$. The value of the He II flux given in Table 1 differs from that of Kaler's due to a narrow slit being used to sample emission along the optically thick axis of the nebula, whereas Kaler's flux refers to that obtained by placing an aperture over the centre region of the nebula. His value is therefore to be prefered as being more representative of the He II flux for the total nebula. The ratio of the continuum flux to that of the flux at 4686 Å then gives a temperature $T_Z(\mathrm{He\ II}) = 118{,}000$ K. The errors in the temperature obtained arise largely due to the errors in the determination of the visual magnitude of the central star. Errors in $T_Z(\mathrm{H})$ and $T_Z(\mathrm{He\ II})$ are $\pm 14{,}000$ K and $\pm 12{,}000$ K respectively.

From the determined Zanstra temperatures a good estimate of the temperature to the central star of NGC 7139 is $T_* = 125{,}000$ K. As a check on this value, a reddened (with $c = 0.6$) blackbody curve, with temperature of 125,000 K, was fitted to the central star IDS spectra. The fit was found to be fair (Fig. 6).

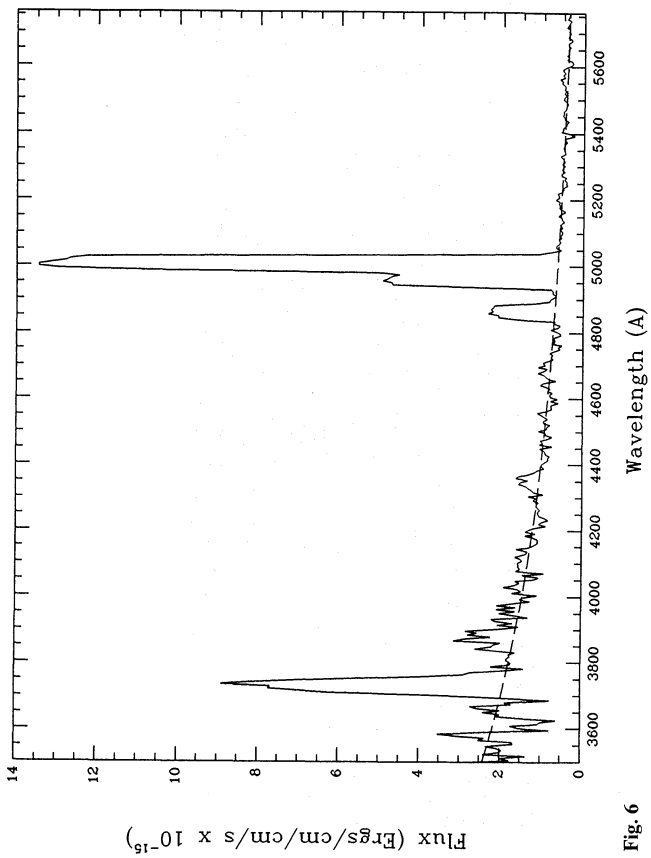

Fig. 6

Fig. 5. This figure shows the profiles of the [O III] 5007 Å (the thick line) and [O II] 3727 Å (the dotted line) emission along the slit obtained from the IDS broad slit spectra. Each channel is 0.″65

Fig. 6. In this plot the fit of a star emitting as a blackbody at 125,000 K (indicated with the dashed line) to the observed flux from the central star (dereddened by $c = 0.6$ and with the nebular continuum subtracted) is shown. The strong emission lines are due to the nebula

Fig. 7. This plot shows the spectra obtained by placing a square aperture of 6.″2 diameter over the centre of NGC 7139 in the [O I] data cube. The peaks at $\approx \pm 40$ km s^{-1} are the [O I] emission from the nebula. The stronger peaks at $\approx \pm 80$ km s^{-1} are due to the [O I] night sky line seen in adjacent orders. The velocity spacing between these two peaks represents the "free spectral range" of the Fabry-Perot

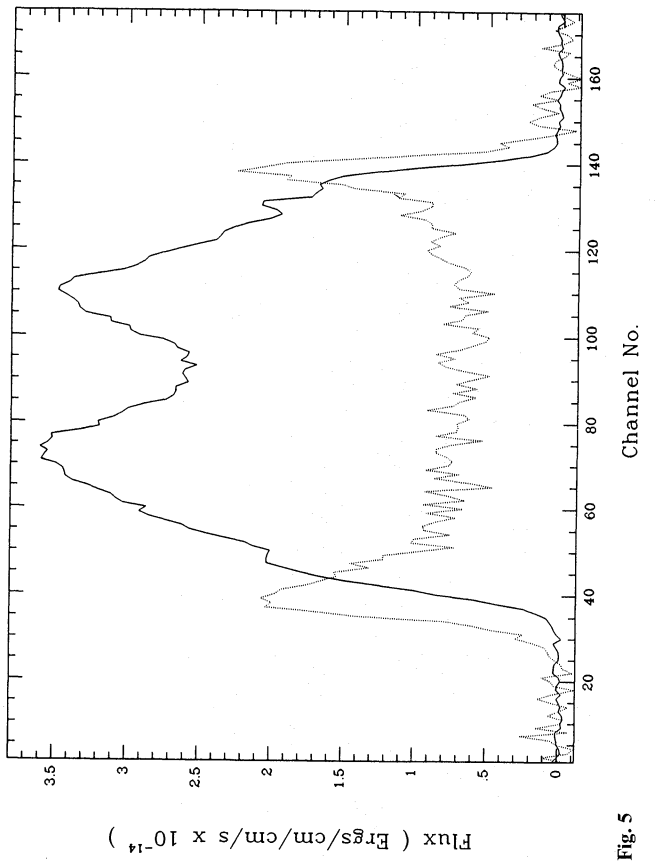

Fig. 5

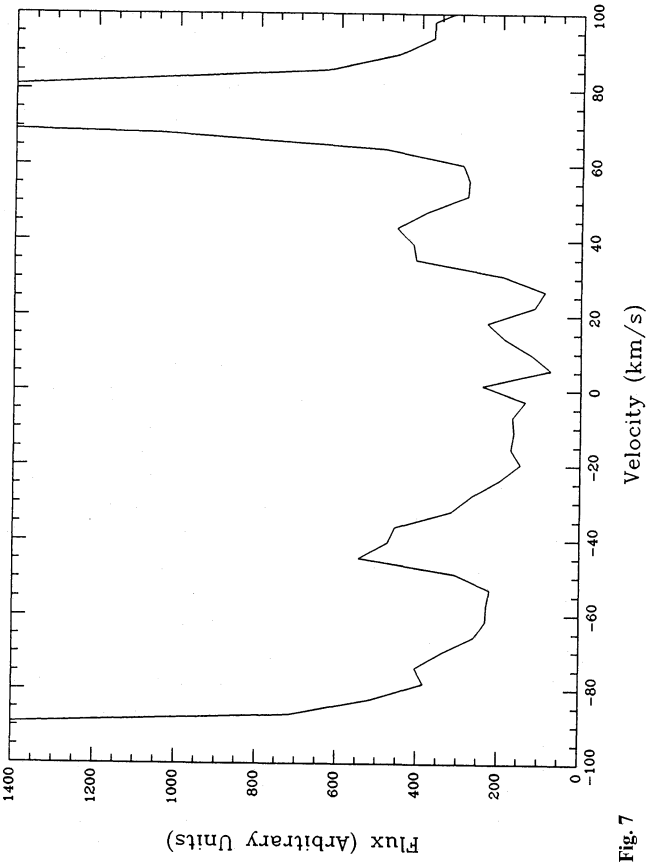

Fig. 7

This temperature is somewhat higher than the estimate of $T = 90{,}000$ K computed by Pottasch (1981) who assumed a brighter centeral star for NGC 7139.

After Pottasch (1981), the stellar radius is computed with the formula:

$$\frac{R_*^2}{d^2} = 1.349\ 10^{-9}\ F_V\ (e^{2.616\times 10^4/T} - 1)$$

Here the distance, d, is measured in cm. F_V is the visual luminosity in erg cm^{-2} s^{-1}. R_* is the stellar radius, also in cm. In this expression V is taken at 5450 Å. Hence, assuming $d = 1.5$ kpc, $R_* = 0.015\ R_\odot$. The luminosity is then about $49\ L_\odot$.

As has been mentioned, distances estimates for NGC 7139 range from 1 kpc to 2.4 kpc. Knowing the Hβ flux from the nebula it is possible to determine its radio flux, $S_{5\,\mathrm{GHz}}$, and hence the ionised mass in the nebula (M_i), which is proportional to $d^{5/2}$, where d is the distance to the nebula. The procedure for calculating the nebula mass is outlined in Gathier (1983). Assuming $d = 1.5$ kpc, then $M_i = 0.169\ M_\odot$ or for $d = 2.4$ kpc, $M_i = 0.549\ M_\odot$. Hence both the mean and upper values for the distance give reasonable values of M_i, the value for 2.4 kpc might be considered as an upper limit.

4. Modelling

4.1. Methodology

In order to better understand the data, model TAURUS data cubes were produced to simulate the observational data. Full details of the modelling technique are to be found in Walsh et al. (1990), and hence only a brief description concerning the model will be given here. The velocity modelling program takes the radial variation of any ionic species, combines this with a velocity law, and computes the integrated emission along the line of sight at each point in the model TAURUS cube. The electron temperature is also considered, the model profile is defined as:

$$B(x,y,v) = \int_{-\infty}^{+\infty} E(x,y,z) \times \exp\frac{-\mathrm{Nm}\,((v - V(x,y,z))^2 + V_T^2)}{2kT(x,y,z)}\,\mathrm{d}z\,.$$

$E(x,y,z)$ is the cube generated on convolution of the geometrical shape for the model with the adopted emission line strength with radius function. $B(x,y,v)$ is the emitted flux, N is the atomic weight of the ionic species, m is the mass of the hydrogen atom, k is the Boltzman constant, $V(x,y,z)$ is the velocity component along the z axis (this being the line of sight). V_T is the turbulent velocity, and $T(x,y,z)$ is the electron temperature. The model cube is generated over the same velocity range as the data. Additionally the theoretical profile is convolved with a Gaussian (to represent the core of the instrumental profile),enabling the model cubes to be directly compared with the TAURUS data.

On examination of the [O I] data (Fig. 3) it is apparent that emission in [O I] is not present (or is only present at a lower level below the noise limit in the observations) at certain positions. The [O III] emission (Fig. 2) is contained within the [O I] emission except at those positions where the [O I] emission is not seen. This suggests that NGC 7139 is not optically thick to Lyman ionising radiation in all directions, as seen from the central star. Hence it was decided to model NGC 7139 in terms of a two component structure, namely an optically thick toroid, the poles of the toroid being considered as optically thin and in effect forming a bicone structure. In our models we were able to alter the angle of inclination of the toroid to the plane of the sky, its position angle on the sky, and the opening angle of the biconical, optically thin sector. A schematic representation of the model is shown in Fig. 4.

Table 1. Line strengths obtained from the broad slit spectrum of NGC 7139

Rest wavelength (Å)	Line ident.	Observed flux Hβ = 100	Dereddened flux Hβ = 100
3727	[O II]	400	565
3870	[Ne III]	45	61
4101	Hδ	27	35
4340	Hγ	40	47
4686	He II	6	6
4861	Hβ	100	100
5007	[O III]	1014	967
5201	[N I]	10	9

From the data, especially considering the [O I] data cube, we could measure the opening angle in the zero velocity frame, between the edges of the east and west bright [O I] rims and the central star; this gives the opening angle for the bicone used in the model. The general velocity law was chosen by considering the observed expansion velocities of the [O I] and [O III] lines at the centre of the nebula. The model which we present uses a linear velocity law of the form: $V(r) = a + k\,r$, where a and k are constants and r is the radius from the central star.

In the computation of these models several important physical parameters describing NGC 7139 are needed as input for the models, namely; the run of electron temperature and density with radius through the nebula, and the ionisation structure of the nebula, especially the run of [O I] and [O III] line strengths as a function of radius. These data can be obtained from a full photo-ionisation model. Unfortunately insufficient spectral data (e.g. for electron density and temperature determinations) are available to produce a realistic photo-ionisation model for this nebula.

However, Clegg et al. (1987) have made a detailed study of the PN NGC 3918. Because of the similarity between NGC 7139 and NGC 3918 in respect of their high central star temperatures, nebular excitation classes, and derived geometrical structures, it was decided to use the variation of [O I] and [O III] line strengths with radius from the photo-ionisation model of NGC 3918 to describe NGC 7139. These were appropriately scaled to account for the differences in sizes of the two nebulae. It was assumed that the electron temperature varied from 12,000 K at the centre of the nebula to 10,000 K at the edge, however the results of the model are rather insensitive to this electron temperature. The electron density is assumed to vary according to the following function:

$$N_H(R) = N_0\,(R/R_1)^n\ \exp(-0.5\,R/R_1)^2),$$

where R_1 is a scale length with the maximum density occurring at $R_1\ n^{1/2}$. It has been shown by Sahu and Desai (1986) that the turbulent velocity in the nebular gas cannot be more than 5 km s^{-1} and hence in producing the velocity model cube we input a turbulent motion of 2 km s^{-1}. The models are insignificantly altered if somewhat larger turbulent motions are assumed.

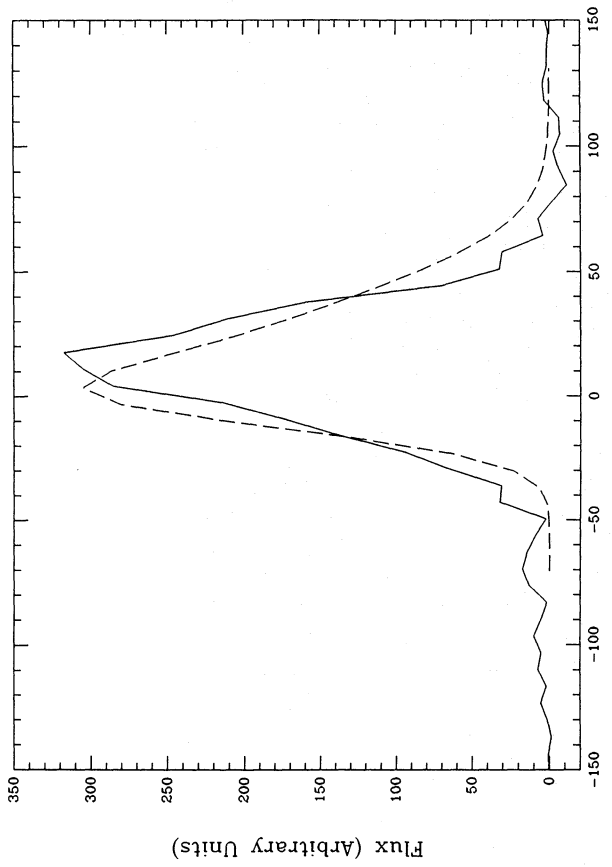

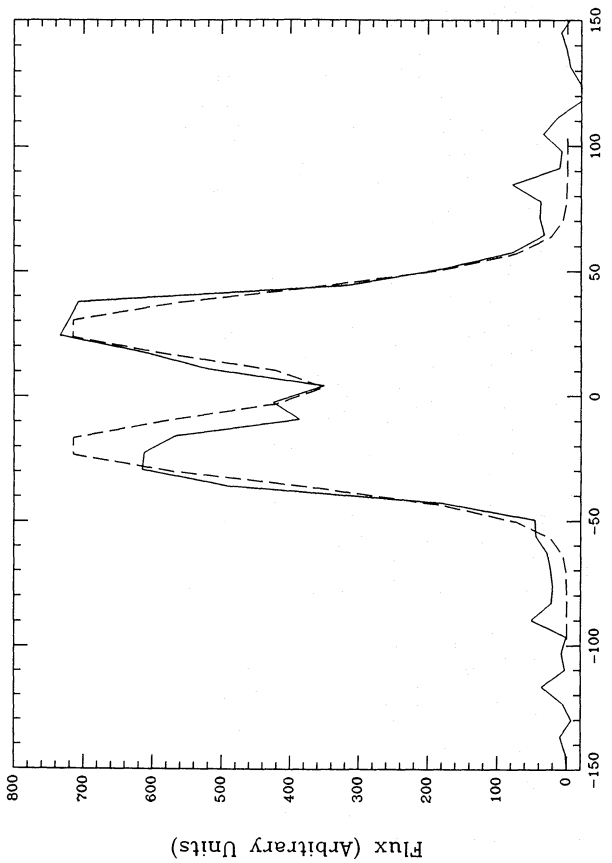

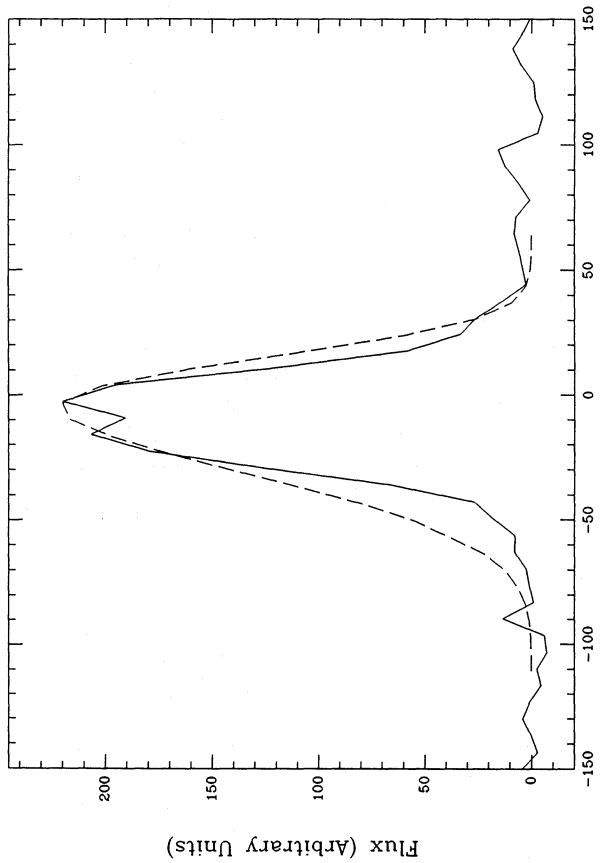

Fig. 8a–c. Comparisons between model and data for the [O III] 5007 Å emission. In these plots the solid line is the data and the dashed line is the model. The relative fluxes shown are on the same scale. **a** shows the spectra obtained by integrating over a square aperture of 2″.9 diameter at the centre of NGC 7139 (position A in Fig. 1b). **b** shows spectra from a 12″.2 diameter aperture placed at position B, as shown in Fig. 1b. **c** is the same as **b** except obtained at position C

Thermal broadening of the line was accounted for taking into account the atomic weight of the ionic species and the electron temperature in the nebula.

4.2. *Comparison with observations*

The availability of TAURUS data in two lines of differing ionisation enabled the velocity law to be determined. The maximum velocity splitting of the two lines, found from the data, was compared with the radius at which the emission peaks, as found from the variation of line strengths with radius output from the photo-ionisation model. This gave the form for the initial velocity law.

The value of the opening angle for the bicone (ψ) was taken to be 70° as determined from the rest velocity RA-Dec frame of the [O I] data cube. The rotation of the bicone on the plane of the sky (ϕ) was also determined from the rest velocity frame and taken to be 30° in the models, this being measured north through east on the sky. Since the [O I] data cube gives information in the outermost regions of the nebula, this was used to determine the angle that the axis of rotation of the bicone subtends with respect to the plane of the sky. This angle (θ) can be expressed as:

$$V_{\text{exp}} \sin\theta = \delta V/2\,,$$

where V_{exp} is the expansion velocity in the [O I] line ($=38\,\text{km s}^{-1}$) and δV is the difference between the observed velocities at the two ends of the bicone ($=40\,\text{km s}^{-1}$, occurring in frames 5 and 11 of the [O I] TAURUS data as seen in Fig. 3). The resultant value of θ is $\approx 30°$, this being used in subsequent trials in generating the model cubes. (However, due to the difficulty in being able to precisely locate the frames at which the ends of the bicone fall, a number of values of θ were tried as outlined below.) The angles θ, ϕ, ψ used to describe the geometry of the models are shown in diagramatic form in Fig. 4.

Initially the same velocity law for both regions was tried, having the form $V(r) = 0 + kr$. The profile taken through the centre of the [O III] model cube matched well the equivalent data profile. At this stage the tilt angle (θ) was varied between $\theta = 15°$ and 45° with the best fit (from matching the RA-Dec frames of model and data) being obtained using $\theta = 30° \pm 5°$. The [O I] data and model profiles were also considered, however due to the lower signal-to-noise in the [O I] data only the [O III] profile comparisons will be discussed further.

It proved impossible with the single velocity law to reproduce the observed velocity shifts from $0\,\text{km s}^{-1}$ seen in the [O III] line profiles taken at positions B and C through the nebula. At this point it was decided to use different velocity laws to describe the optically thin and thick parts of the nebula. It is plausible that the material in the optically thin part of the nebula is able to expand at greater velocities than that in the optically thick part of the nebula due to the lower densities present. Hence the form of the velocity law for the "thin" part was taken to be the same as that for the "thick" part expect that $k_{\text{thin}} = 2.5\,k_{\text{thick}}$. The value of the constant k was $k_{\text{thick}} = 165\,\text{km s}^{-1}\,\text{pc}^{-1}$. The value of 2.5 was derived by comparing the velocity shift of the profiles taken at positions B and C for the data and the model (single velocity law). Figure 8 shows the observed profiles taken at positions A, B, and C along with the corresponding model predictions. The fit for the profile taken at the centre of the nebula (A) is excellent, the fits for positions B and C are reasonable.

It might be noted that a velocity law in which the velocity decreases as a function of distance from the central star was found to be impossible. This is due to the constraints set by the observed expansion velocities in [O I] and [O III] from profiles taken through the centre of the nebula, and the distance from the centre of the nebula at which the [O I] and [O III] emission is seen to peak.

From the final model TAURUS data cubes the individual RA-Dec frames could be extracted and directly compared with the corresponding RA-Dec frames from the observational data. Care was taken to ensure that the velocity interval over which the model frames were summed was equivalent to the data frames. In Figs. 2b and 3b the individual RA-Dec frames from the [O III] and [O I] model respectively are presented. As in the data (shown above in the same Plates) the frames go from red to blue on viewing from top left to bottom right. It can be seen from the comparison of model with observations that the qualitative fit is rather good.

Firstly the [O I] data will be considered. The variation of the bright rims seen in the [O I] data with velocity is well represented in the model. Specifically the change in size and position of the "hole" in [O I] emission with velocity in the observations (seen to go from the NE of the nebula at receding velocities to SW at approaching velocities) is matched by the model. In a similar fashion the [O III] model reasonably reproduces the observations. The [O III] emission from the model also lies within the [O I] model emission, as seen in the observations. The "cusps" which are seen at the outer velocities in both the [O I] and [O III] data cubes are well matched in both position and shape by the corresponding model cubes. For example, the "cusp" seen in the [O III] data in Fig. 2a, top right frame, is matched by the equivalent model frame in Fig. 2b. However, as can be seen, the emission from the interior of the [O III] model is a poor match to the data, this being a consequence of the fact that some of the input parameters to our velocity model were obtained from the photo-ionisation model for NGC 3918. Using the [O III] ion strength as a function of radius from a full photo-ionisation model for NGC 7139, as input into the velocity models, could be expected to result in a better match, model to data, of the distribution of [O III] emission in the inner regions of the nebula.

5. Discussion

From the "direct" images (see Fig. 1) NGC 7139 appears as a basically round nebula with a major diameter of $\approx 70''$. The [O I] emission is localised in a thin shell at the outer edge of the nebula, with the emission being brightest along the east and west rims. The [O III] emission is contained within the [O I] emission, peaking somewhat closer to the central star and has a bipolar appearance. However, faint emission in [O III] is seen along the axis at 30° to north, extending outside the [O I] emission in just the regions where the [O I] emission is faintest. This is probably evidence that the nebula is not ionisation bounded in all directions, and that low density, higher temperature material is expanding into the inter-stellar medium. This is seen as the faint [O III] emission. The (pseudo) narrow band image shown in Fig. 1a would suggest that the [O I] emission along the rims is at a ionisation-shock front indicating that in this region the nebula is ionisation bounded. Further evidence for this is provided by the IDS data (Fig. 5) where the [O II] emission peaks further out in the nebula than does the [O III] emission.

As mentioned earlier, when determining the central star temperature with the Zanstra method, the surrounding nebula is assumed to be optically thick to Lyman ionising radiation (or optically thick in the He II Lyman continuum if using the He II Zanstra method). The work presented here shows that NGC 7139 is optically thin in some directions to Lα radiation. Hence the

temperature for the central star determined by the Zanstra method is an underestimate of the true effective temperature of the central star. This has also been found to be the case for NGC 3918 (Clegg et al., 1987), another nebula modelled in terms of an optically thin and an optically thick structure.

In the above sections the best fit model to the data has been presented. However to determine the reasonableness of the velocity law in the model, other model TAURUS cubes having velocity laws representative of different possibilities were tried. In one, the velocity law was taken to show the case where there was a positive velocity at the central star, i.e. $V(r) = 10 + k' r$ and one with a negative velocity at $r = 0$ i.e. $V(r) = -5 + k'' r$. These were found to give a less good fit to the observed data in particular with regard to the position of the opening of the [O I] rims in the RA-Dec frames.

It is important to note that this model may not be the unique solution. However this is the simplest model which can be shown to reproduce the large scale structure which is seen in the kinematical data for NGC 7139. This model is unable to account for some of the smaller scale structure seen, but in view of some of the simplifications inherent in the model this is perhaps unsurprising. With a more accurate knowledge of some input parameters, to be obtained from a full photo-ionisation model for NGC 7139, improvements in the fit could be expected. It is satisfying that this fairly simple model is able to match the data, and this confirms the suggestion (Clegg et al., 1987) that biconical structures, viewed from varying angles, may explain a large proportion of the structures seen in planetary nebulae.

The model for NGC 7139 shows that different velocity laws are valid for the optically thick and thin sectors. An interesting point is if this information enables us to discriminate between various scenarios for PN formation. The higher velocities seen in the optically thin material may indicate that the precursor asymptotic giant branch (AGB) wind or superwind had velocities differing with ejection direction. Alternately the AGB wind may have been isotropic, then at a later stage variations in the fast stellar wind from the central star of the PN may have acted so as to preferentially accelerate the optically thin part of the nebula. A further possibility is that the higher velocity material seen in the optically thin sector of NGC 7139 is evidence for a spherically symmetric fast wind from the central star having interacted with a non-spherically symmetric wind from the precursor, following the scheme outlined by Balick et al. (1987).

One theory of the formation of planetary nebulae is the so called "interacting winds" model (Kwok et al., 1978; Volk and Kwok, 1985). In this the fast wind from the central star (with a velocity of $\sim 2000\,\mathrm{km\,s^{-1}}$ and a mass-loss rate of $\sim 10^{-7}$ to $10^{-8}\,M_\odot\,\mathrm{yr^{-1}}$) drives a shock into the former red giant envelope (RGE) deposited by the slow wind from the planetary nebula precursor (with a velocity of $\sim 10\,\mathrm{km\,s^{-1}}$ and a mass-loss rate of $\sim 10^{-4}$ to $10^{-5}\,M_\odot\,\mathrm{yr^{-1}}$). This model is a one dimensional model and has been shown to successfully account for the appearance of spherically symmetric PN (e.g. Balick, 1987).

However there are a large number of PNe which show features that can not be explained by the simple 1-D wind model. NGC 7139 is one of these, showing evidence for biconical structure. Balick et al. (1987) have proposed a modification to the basic 1-D case in which the "fast" central star wind interacts with a non-spherically symmetric RGE. The non-symmetry of the RGE may be caused by similar physical mechanisms as those that are thought to be involved in mass loss from early type stars (i.e. Poe and Friend, 1986). One prediction of the Kwok et al. model is that the nebula velocity is independent of radius. In the case of NGC 7139 this is not the case. Hence, it is possible that the adapted 2 wind interacting model is insufficient to explain NGC 7139.

Schmidt-Voigt and Köppen (1987) have proposed a 3-wind model for PN formation. Here there is a normal "Reimers"-type wind, a "superwind" (both stages occurring during the AGB stage of the stars evolution) and a later fast wind from the PN central star. They show expected expansion velocity-nebular radius plots for the case of 2-wind and 3-wind models for nebular evolution. The 3-wind models have the velocity of expansion of the nebular gas increasing with radius, although the "accreting" 3-wind model (i.e. where significant material from the AGB is accreted and hence the density in the nebula increases towards the outer radius in the final stages of the PN evolution) shows an expansion velocity which stays constant beyond a certain radius. The relatively high expansion velocity seen in NGC 7139, $V_{\mathrm{exp}} = 38\,\mathrm{km\,s^{-1}}$ in [O I], together with the $V \propto r$ velocity law would seem to indicate a 3-wind model can be used to explain the evolution of this nebula. To study this further it is necessary to gain information on the ionised nebular mass from optical and radio data. Additionally it would be helpful to know whether there is in fact a fast central star wind (and if so what the mass loss rate is) from the central star of NGC 7139. Detection of P-Cygni profiles of UV lines (e.g. [O V]) gives direct evidence of a fast stellar wind. However this star is too faint to be measured by the IUE satellite and hence will have to await HST observations.

With a knowledge of the velocity law for NGC 7139 the kinematic age of the nebula can be found. The distance to the nebula is taken as 1.5 kpc. The diameter of the optically thick section of the nebula is $\approx 70''$. The velocity law is $V_{\mathrm{exp}} = k r$ where $k = 165\,\mathrm{km\,s^{-1}\,pc^{-1}}$. Hence the kinematic age of the nebula is 5925 yr. It is interesting to compare this with the ages of 6560 yr and 8910 yr that are obtained if the velocity in the entire nebula is taken as $V_{\mathrm{exp}} = 38\,\mathrm{km\,s^{-1}}$ for [O I] and $V_{\mathrm{exp}} = 28\,\mathrm{km\,s^{-1}}$ for [O III] respectively. Hence it is apparent that the choice of velocity law is an important consideration when determining nebular kinematic ages, in this case affecting the result by some 10% to 30%.

The values for the temperature and luminosity of the central star of NGC 7139 are $\log T = 5.09$ and $\log L = 1.69$. The central star can be placed on the H-R diagram and its position compared with theoretical evolutionary tracks for central stars of various masses. Using for example the tracks of Wood and Faulkner (1986) we see that the central star of NGC 7139 has a mass of $\approx 0.8\,M_\odot$. The theoretical evolutionary time scale for the central star to have evolved to this point is over 30,000 yr. However the nebula's kinematic age has been shown to be ≈ 6000 yr. There is obviously some cause for concern in this lack of agreement.

6. Conclusions

In this paper TAURUS observations of NGC 7139 in [O I] 6300 Å and [O III] 5007 Å have been reported. A geometrical model has been made which is able to reproduce the main velocity structure seen in NGC 7139. The model has two components, namely a toroidal optically thick section and a smaller biconical region where the nebula is optically thin to Lyman ionising radiation. A consequence of this is that the Zanstra method, as used to determine the central star temperature, will give an underestimate of the true temperature. The expansion velocity law is determined as $V_{\mathrm{exp}} = k r$ where $k = 165\,\mathrm{km\,s^{-1}\,pc^{-1}}$ for the optically thick part of the nebula and $k = 410\,\mathrm{km\,s^{-1}\,pc^{-1}}$ for the optically thin biconical section of the nebula.

Acknowledgements. We would like to thank the staff of the La Palma observatory and especially Dr. S. Unger, for their help. The Isaac Newton Telescope at La Palma is operated by RGO at the Observatorio de los Muchachos of the Instituto Astrofisico de Canarias. The help of A. Schoenmaker in phase correcting the data is gratefully acknowledged. NAW was supported by an NATO/SERC fellowship for the duration of this work. JRW was supported by a Royal Society European Visiting Fellowship.

References

Allen, R.J., Ekers, R.D., Terlouw, J.P.: 1985, in *Proc. Intern. Workshop on Data Analysis in Astronomy at Erice*, eds. L. Scarci, V. di Gesu, Plenum, London

Amnuel, P.R., Guseinov, O.H., Rustanov, Y.S.: 1989, *Astrophys. Space Sci.* **154**, 21

Atherton, P.D., Taylor, K., Pike, C.D., Harmer, C.F.W., Parker, N., Hook, R.N.: 1982, *Monthly Notices Roy. Astron. Soc.* **201**, 661

Balick, B.: 1987, *Astron. J.* **94**, 671

Balick, B., Preston, H.L., Icke, V.: 1987, *Astron. J.* **94**, 1641

Bohuski, T.J., Smith, M.G.: 1974, *Astrophys. J.* **193**, 197

Boksenberg, A.: 1972, *Auxiliary Instrumentation for Large Telescopes*, ESO/CERN Conference, Geneva, p. 205

Cahn, J.H.: 1984, *Astrophys. J.* **279**, 304

Clegg, R.E.S., Harrington, J.P., Barlow, M.J., Walsh, J.R.: 1987, *Astrophys. J.* **314**, 551

Gathier, R.: 1984, Thesis, The University of Groningen

Jacoby, G.H., Hunter, D.A., Christian, C.A.: 1984, *Astrophys. J. Suppl. Ser.* **56**, 257

Kaler, J.B.: 1976, *Astrophys. J. Suppl. Ser.* **31**, 517

Kwok, S., Purton, C.R., FitzGerald, P.M.: 1978, *Astrophys. J.* **219**, L125

Mulder, P.S., Schoenmaker, A.A., Valentijn, E.A.: 1988, *Report on the 125 micron etalon of TAURUS II*, Technical Note, Kapteyn Sterrenwacht, Roden

O'Dell, C.R.: 1963, *Astrophys. J.* **138**, 293

Pilyugin, L.S., Khromov, G.S.: 1979, *Soviet. Astron.* **23**, 425

Poe, C.H., Friend, D.B.: 1986, *Astrophys. J.* **311**, 317

Pottasch, S.R.: 1981, *Astron. Astrophys.* **94**, L13

Reay, N.K., Atherton, P.D.: 1985, *Monthly Notices Roy. Astron. Soc.* **251**, 233

Reay, N.K., Atherton, P.D., Taylor, K.: 1983, *Monthly Notices Roy. Astron. Soc.* **203**, 1079

Sabbadin, F.: 1984, *Astron. Astrophys. Suppl. Ser.* **58**, 273

Sabbadin, F., Ortolani, S., Bianchini, A.: 1985, *Monthly Notices Roy. Astron. Soc.* **213**, 563

Sahu, K.C., Desai, J.N.: 1986, *Astron. Astrophys.* **161**, 357

Schmidt-Voigt, M., Köppen, J.: 1987, *Astron. Astrophys.* **174**, 223

Stone, R.P.S.: 1977, *Astrophys. J.* **218**, 767

Taylor, K., Atherton, P.D.: 1980, *Monthly Notices Roy. Astron. Soc.* **191**, 675

Tüg, H., White, N.M., Lockwood, G.W.: 1977, *Astron. Astrophys.* **61**, 679

Volk, K.M., Kwok, S.: 1985, *Astron. Astrophys.* **1985**, 79

Walsh, J.R., Sahu, K.C., Clegg, R.E.S.: 1990 (in preparation)

Wamsteker, W.: 1981, *Astron. Astrophys.* **97**, 329

Weinberger, R.: 1989, in *Planetary Nebulae*, *IAU Symp.* **131**, ed. S. Torres-Peimbert, Reidel, Dordrecht, p. 93

Weinberger, R., Ziener, R.: 1988, *Astron. Astrophys.* **191**, 297

Weedman, D.W.: 1968, *Astrophys. J.* **153**, 49

Wilson, O.C.: 1950, *Astrophys. J.* **111**, 279

Wilson, O.C.: 1958, *Rev. Modern Physics* **30**, 1025

Wood, P.R., Faulkner, D.J.: 1986, *Astrophys. J.* **307**, 659